Manuscript prepared for The Cryosphere
with version 2014/09/16 7.15 Copernicus papers of the LaTeX class copernicus.cls.
Date: 5 December 2017

~~Stable accumulation~~ Accumulation patterns around Dome C, East Antarctica, ~~over~~ in the last ~~glacial cycle~~73 kyrs

Marie G.P. Cavitte[1,2], Frédéric Parrenin[3], Catherine Ritz[3], Duncan A. Young[1], Brice Van Liefferinge[4], Donald D. Blankenship[1,2], Massimo Frezzotti[5], and Jason. L. Roberts[6,7]

[1]Institute for Geophysics, Jackson School of Geosciences, University of Texas at Austin, Austin, Texas, USA
[2]Department of Geological Sciences, Jackson School of Geosciences, University of Texas at Austin, Austin, Texas, USA
[3]Univ. Grenoble Alpes, CNRS, IRD, IGE, F-38000 Grenoble, France
[4]Laboratoire de Glaciologie, Université libre de Bruxelles, CP 160/03, Avenue F.D. Roosevelt 50, B-1050 Brussels, Belgium
[5]ENEA, Agenzia Nazionale per le nuove tecnologie, l'energia e lo sviluppo sostenibile, Rome, Italy
[6]Australian Antarctic Division, Kingston, Tasmania 7050, Australia
[7]Antarctic Climate & Ecosystems Cooperative Research Centre, University of Tasmania, Hobart, Tasmania 7001, Australia

Correspondence to: Marie G.P. Cavitte (mariecavitte@gmail.com)

Abstract. We reconstruct the pattern of surface accumulation in the region around Dome C, East Antarctica, ~~through~~ since the last glacial~~cycle~~. We use a set of ~~internal isochrones~~ 18 isochrones spanning all observable depths of the ice column interpreted from various ice-penetrating radar surveys and a 1D pseudo-steady ice flow model to invert for ~~both~~ time-averaged accumulation rates ~~and~~ in the region. The shallowest four isochrones are then used to calculate paleoaccumulation rates between isochrone pairs using a 1D assumption where horizontal advection is negligible in the time interval of each layer. We observe that the ~~surface accumulation pattern is~~ large-scale (100s km) surface accumulation gradient is spatially stable through the last ~~128 kyrs, both the large-scale (100s km) gradients which reflect~~ 73 kyrs, which reflects current modeled and observed precipitation gradients in the region~~, as well as the~~. We also observe small-scale (10s km) accumulation variations linked to snow redistribution at the surface due to changes in its slope and curvature in the prevailing wind direction ~~. This suggests a stable position of the dome throughout the last glacialcycle~~that remain spatially stationary since the last glacial.

1 Introduction

The Dome C region, located on the East Antarctic interior plateau, has long been the focus of extensive research: it is the site of the oldest as-yet-retrieved continuous ice core, the EPICA Dome C ice core, going back ~800 ka ~~(?). It is also an area where surface precipitation~~ (?). Modern

surface precipitation on the Dome C plateau is extremely low ~~(?). At other inland plateau sites (e.g. in Drönning Maud Land, ?), occasional large precipitation events represent a large part (~~(~25 mm yr^{-1}, ?), with infrequent storm events representing more than 50% ~~)~~ of the total annual precipitation ~~, and this is the case at Dome C too (?). Precipitation on the Dome C plateau is mostly dominated by coastal air masses which advect moisture inland. The presence of the dome creates an upslope and a downslope component of air flow: moisture is released preferentially on the upslope/windward side of the dome, and the leeward/downslope side is therefore exposed to drier air (?). This is reflected in the large scale gradient of modern precipitation measured (???) and modeled (???).~~

~~Although observations and model results suggest a spatially variable shift in dust particle sizes, they indicate a uniform geographic provenance for mineral dust measured at EPICA Dome C~~ (?). ~~An efficient and persistent westerly circulation pattern would have transferred dust from South America and Australia to the East Antarctic plateau during glacial-interglacial cycles (??).~~ Coastal air masses lose moisture as they are driven inland to higher elevation, resulting in a characteristic precipitation gradient with higher measured and modeled precipitation on the north side of Dome C (??????). Present-day moisture-bearing air mass trajectories (??) point to a western Indian Ocean provenance for the snow precipitation at Dome C (85% of the precipitation), and suggest this could have persisted through glacial-interglacial cycles.

Snow precipitation is homogeneous at a large-scale, whereas local variations in snow accumulation are controlled by local surface topography as a function of wind direction. ? and ? ~~first observed~~ are the first to observe the close relationship between bedrock relief, surface slope and accumulation rates in Wilkes Land. ? details how wind speed and direction can affect total mass balance in Marie Byrd Land. ? show that surface slope in the prevailing wind direction (SPWD) is a key constraint in determining spatial and temporal variability of precipitation; a higher SPWD can lead to significant ablation and redeposition of snow (????). ? show that SPWD is a strong threshold for the formation of wind scour or megadune fields. Evidence for a persistent westerly wind circulation pattern comes from mineral dust measured at EPICA Dome C which shows a uniform geographic provenance from South America and Australia to the East Antarctic plateau during glacial-interglacial cycles (??).

Airborne and ground-based ice-penetrating radar data have long been used to constrain the surface and bedrock topography over large parts of the Antarctic Ice Sheet (?????, and many others), as well its internal stratigraphy ~~(???)~~(e.g. ???). Because the internal stratigraphy represents isochronal surfaces throughout much of the ice sheet, dated internal radar reflectors can be used to directly constrain the surface mass balance of the ice sheet ~~(?).~~ in the highest part of the ice column (??). Reconstructing accumulation history from deeper isochrones is more ill-posed as both accumulation variations and changes in ice flow can affect isochrone geometries (e.g. ??????), and assumptions have to be made about one or the other (????, see companion paper for more discussion). Assumptions on the vertical strain rate will also affect reconstructed paleoaccumulation rates (e.g. ??, etc.). Several radar isochrone studies have ~~also~~ shown the existence of a coast-to-dome precipitation gradient:

? show a continuous existence ~~through historical timescales~~of a precipitation gradient through the last 300 years, while **?** shows the persistence of a strong accumulation gradient between Dome C and Ridge B (a topographic high upstream of Lake Vostok) over glacial-interglacial timescales.

~~The position of Dome C and the adjacent ice divide have been presumed to be stable through time . However, there is no reason that this should be the case: bounded to the east by the Byrd Glacier catchment and to the west by the Totten Glacier catchment, these two glaciers have very different flow behaviors due to different outflow and grounding line boundary conditions and therefore might have influenced Dome C in an asymmetrical way. Shrinking of the stabilizing Ross Ice shelf on the Byrd Glacier catchment side has been observed and modeled (???), and ? have shown evidence for significantly different configurations of the Totten Glacier catchment over long time-scales. There is potential for the dome to have migrated or disappeared over time to simply become part of the ice ridge if the glaciers destabilized at different times. Knowing the position of the dome is crucial for three~~ Better constraining accumulation rates through time is important for several reasons:

1. The ~~position of topographic domes characterizes the~~ spatial distribution of snow accumulation ~~and the ice flow of outlet glaciers of the East Antarctic Ice Sheet (EAIS). Mass balance strongly affects sea level variations (past and future) as well as~~ affects the position of topographic domes, which ultimately affects the geometry of the ice sheet ~~through time. Several recent studies have shown the influence of increasing precipitation trends over Antarctica in a warming climate (???).~~ (with its resulting sea-level implications) through time (**???**).

2. ~~The position of the dome through time is~~ In addition to other parameters, accumulation rates are required for accurate dating and interpretation of ice cores. ~~Knowing the flowlines~~ Constraints on accumulation and flowline geometries of ice particles through time ~~is~~ are necessary to reconstruct ice core chronologies and correct for the effects associated with deposition at a different location and elevation than the ice coring site (**??**). Especially in the context of the search for 1.5 million-year-old ice, ~~knowing the position of the dome through time~~ such constraints will have a significant influence on the choice of an ice core site. ~~Several candidate sites for such old ice have been identified in the region (?).~~

3. The ~~location of the dome is required to model isochrones interpreted from radar surveys. When modeling isochrones, the assumption that horizontal advection is negligible is only valid in close proximity to a dome or ice divide. If this is not the case, full 3D-type modeling with known dome and divide positions is necessary to reproduce isochrone geometries accurately (??)~~temporal evolution of accumulation rates provides important constraints on ice sheet mass balance through time for modeling experiments (**??**).

Here, we reconstruct paleoaccumulation rates for the Dome C region using a 1D pseudo-steady ice flow model ~~(described in the companion paper)~~ (described in the companion paper: **?**) for the last ~~128~~ 73 kyrs using the isochronal constraints obtained from radar surveys. We discuss the large-

scale accumulation and small-scale variations in accumulation ~~which suggest a stable position of the dome for the last glacial cycle~~calculated around Dome C. We do not attempt to reconstruct ~~older paleoaccumulations~~ paleoaccumulation further back in time due to the 1D assumptions and the increasing horizontal advection with depth.

2 Methods

2.1 Dome C region

The Dome C region represents a topographic high in the middle of the EAIS and is at the confluence of several ice divides, the largest of which separates the Byrd Glacier catchment from the Totten Glacier catchment. The topography ~~is gentle~~of the Dome C region is gentle: the change in elevation is ~10 m across 50 km (**?**), reaching a maximum elevation at Dome C of ~3266 m above sea level (geoid height)~~where the change in elevation is ~10 m across 50 km (?). A gentle~~ . A saddle connects Dome C to Lake Vostok along the ice divide, with a secondary dome referred to as "Little Dome C" (LDC) just south of the Dome C ice core site. The bedrock is characterized by a large subglacial massif ~40 km to the south of the Dome C ice core site and ~10 km south of the LDC, easily identifiable on Fig.1, where the radar survey grid is tightest. For ease of description, we refer to it as the "Little Dome C ~~massif" (LDCm~~Massif" (LDCM) to differentiate from the surface topographic high. The deep Concordia Subglacial Trench (CST) runs along its eastern edge and is followed by a steep ridge, ~2000 meters high (**?**), which we will refer to as the Concordia Ridge (CR). Both the ~~LDCm~~ LCDM and the CR (see Fig.1) have been identified as promising targets for retrieving 1.5 million-year old ice (**?**).

2.2 Radar data

We use several airborne ice-penetrating radar surveys collected in the Dome C region by the University of Texas at Austin Institute for Geophysics (UTIG) and the Australian Antarctic Division (AAD) as part of the ICECAP project (International Collaborative Exploration of the Cryosphere through Airborne Profiling, **?**) and the Oldest Ice candidate A (OIA) survey flown by ~~ICECAp~~ ICECAP in January 2016 ~~(?) (Fig. 1).~~ (Fig.1, **?**). All surveys use the same center frequency of 60 MHz~~; internal isochrones are therefore coherent~~ , and the same bandwidth of 15 MHz; radar isochrones can therefore be easily matched from one season to the next. A set of 18 ~~internal~~ isochrones are traced throughout the region, using ~~the~~ multiple crossovers, thus ensuring the reliability of the tracing as outlined in **?**. The co-location of the EPICA Dome C ice core in the survey region enables the dating of the isochrones using the AICC2012 chronology (**??**). Obtaining ages and associated uncertainties for each isochrone is described in **?**. We extend the same isochrones to the newly acquired OIA survey and add a number of shallower and deeper isochrones in the OIA region (Cavitte et al., in prep.). We use all 18 isochrones for the 1D model inversion but only use the youngest ~~nine~~ four isochrones

going back ~~to the penultimate interglacial (i.e. 128~~ into the last glacial (10 - 73 ka) for paleoaccumulation reconstructions, explained below. All ~~nine~~ four isochrone depths, ages and uncertainties at the Dome C ice core site are given in Table 1.

2.3 Modeling

We use 18 radar isochrones, dated from 10 ka (before 1950) to 366 ka, and the 1D pseudo-steady ice flow model described in the companion paper (**?**). The model inverts for time-averaged geothermal heat flux (G_0), time-averaged accumulation rate ($\bar{a}$), and time-averaged vertical strain rate profile parameter (p') every kilometer along a radar line. Pseudo-steady-state means that all parameters in the model are considered steady except for $R(t)$, a temporal factor applied to both basal melting and accumulation (see companion paper). In other words, we can split the accumulation rate into a time-averaged component $\bar{a}(x)$ that varies spatially, and a temporally varying component, $R(t)$:

$$a(x,t) = \bar{a}(x)R(t) \tag{1}$$

$\bar{a}(x)$ therefore is the time-averaged accumulation rate at a certain point x, while $R(t)$ represents the variations in accumulation rate over glacial-interglacial cycles over time. The model assumes that $R(t)$ is spatially invariant over the entire study region. $R(t)$ is obtained from AICC2012 inferred accumulation variations (**??**), and represents the ratio of the accumulation at time t to the average accumulation over the last 800 kyrs.

When inverting the radar isochrones using the pseudo-steady ice flow model, ages and accumulations are all used in steady-state form, with glacial-interglacial accumulation variations normalized. The calculated time-averaged accumulation rate $\bar{a}$ (Fig.3), p', and G_0 result from the best fit of all the radar isochrone depths (dropping x for simpler notation). However, some differences between modeled and observed isochrones remain as all isochrones have to be simultaneously fitted for each point x. The 18 isochrones have to be used in the inversion as the deepest isochrones provide the strongest constraints on p' and G_0.

To reconstruct paleoaccumulation rates through time $\bar{a}_{\Delta\chi}$, where $\Delta\chi$ represents a discrete age interval, we use the G_0 and p' values calculated and assume they remain unchanged over each time so that the remaining misfit between modeled and observed isochrones is entirely a result of the uncertainty in $\bar{a}$. $\bar{a}_{\Delta\chi}$ represents the time-averaged paleoaccumulation rate for a layer with an age interval $\Delta\chi$, bounded above and below by a radar isochrone of AICC2012 age. We refer to these as isochrone-bounded layers. To calculate $\bar{a}_{\Delta\chi}$ values for each layer, we adjust the value of $\bar{a}$ such that modeled and observed isochrone-bounded layer age intervals $\Delta\chi$ are fitted perfectly for each layer.

In mathematical form, if z is the depth of the isochrone and χ the age of the isochrone, we can write the isochrone-bounded layer's age interval ~~as:~~ in steady-state form as:

$$\Delta\chi_{m}^{steady} = \frac{\Delta z}{\tau \bar{a}_{m,\Delta\chi}} \text{ , for the model} \int_{z_1}^{z_2} \frac{dz}{\tau(z)\bar{a}_{m,\Delta\chi}} \text{ , for the model,} \tag{2}$$

and

$$\Delta\chi_o^{steady} = \frac{\Delta z}{\tau \bar{a}_{o,\Delta\chi}} \int_{z_1}^{z_2} \frac{dz}{\tau(z)\bar{a}_{o,\Delta\chi}} \text{, for observations,} \quad (3)$$

where τ ~~represents~~ is the vertical thinning ~~rate. We therefore~~ function, i.e. the ratio of the vertical thickness of a layer to its initial vertical thickness at the surface, and $\Delta\chi^{steady}$ is the steady-state age interval $\Delta\chi$ using Eq.1.

We want to obtain $\bar{a}_{o,\Delta\chi}$, the "observed" paleoaccumulation rate for a certain age interval $\Delta\chi$. This is similar to the "shallow-layer approximation" used by **?**.

Assuming all errors arise from the accumulation rate uncertainty is equivalent to assuming τ is modeled perfectly. Therefore we can equate Eq.2 with Eq.3 and obtain $\bar{a}_{o,\Delta\chi}$:

$$\bar{a}_{o,\Delta\chi} = \frac{\Delta\chi_m}{\Delta\chi_o} \frac{\Delta\chi_m^{steady}}{\Delta\chi_o^{steady}} \bar{a}_{m,\Delta\chi} \quad (4)$$

Using Eq.4, we calculate the best fit time-averaged paleoaccumulation rates through time in one iteration after the model inversion. The values of $\bar{a}_{o,\Delta\chi}$ obtained are the time-averaged paleoaccumulation for each isochrone-bounded layer of age interval $\Delta\chi$. This gives the spatial variations of the paleoaccumulation rates through time.

To respect our assumption that τ is modeled perfectly, we only calculate paleoaccumulation rates $\bar{a}_{o,\Delta\chi}$ for the first four isochrone-bounded layers. Our fourth and deepest layer used reaches an average depth of 30% of the ice thickness, with calculated thinning never reaching below 0.6. Furthermore, to avoid ill-posed conditions for our 1D paleoaccumulation reconstructions, we only retain data points that have experienced a maximum of 5 km of horizontal advection. We do this for each layer, using **?** ice surface balance velocities, corrected for temporal velocity variations using $R(t)$ (**?**), and the age interval spanned by the layer considered. Any point that has traveled more than 5 km horizontally is masked.

Temporal variations $R(t)$ of the accumulation rates have been ignored until this point. We use Eq.1 and calculated $R(t)$ values from the AICC2012 chronology accumulation variations to obtain the corresponding paleoaccumulation rates, $a_{o,\Delta\chi}$. ~~These are shown~~ We show the paleoaccumulation rates calculated for the four youngest age intervals spanning 0 - 73 ka in Fig.2 and 4.

~~In addition, the~~ Care must be taken in not over-interpreting the paleoaccumulation maps obtained. We do not argue that we have reconstructed absolute paleoaccumulations for the past 73 kyrs. The 1D pseudo-steady ice flow model used here (see companion paper, **?**) does not take horizontal advection into account. Paleoaccumulation rates calculated are valid at the ice divide and the dome where horizontal ice flow speeds are negligible. Farther away, horizontal advection has a larger influence. A full 3D model is required to reconstruct accumulation rates more extensively in space and further in time.

The Metropolis-Hastings (MH) algorithm (described in the companion paper, **?**) enables the calculation of an accumulation rate uncertainty which takes into account the age uncertainty of the radar isochrones (see S2). The age uncertainty of the radar isochrones is a combination of the radar depth uncertainties translated to age uncertainties (**?**) and the AICC12 ice core chronology uncertainties (**??**). **?** describe the various sources of radar depth uncertainty and how they are calculated. The radar isochrone depth and age uncertainties are given in Table 1. We plot the time-averaged accumulation rate and the paleoaccumulation rates for each isochrone-bounded layer over the survey region (see Fig.3, 4). The accumulation rate uncertainties are given in Fig. S2 ~~.~~ and further discussed in Supplement 2.

~~Care must be taken in not over-interpreting the paleoaccumulation maps obtained. We do not argue that we have reconstructed absolute paleoaccumulations for the past 128 kyrs. The 1D pseudo-steady ice flow model used here (see **?**) does not take horizontal advection into account. Instead, our paleoaccumulations are valid at the ice divide and the dome where horizontal ice flow speeds are negligible. Farther away, horizontal advection has a larger influence. We therefore focus on the OIA survey, which is closest to the dome, augmented only by radar lines from previous seasons nearest to the ice divide (**??**). Our paleoaccumulation calculations do not apply deeper in the ice column where the assumption that τ (Eq.4) is fitted perfectly breaks down. We therefore reconstruct paleoaccumulation rates only over the last glacial cycle, and use the topmost nine isochrones which cover the period 10 - 128 ka (top half of the ice column). Furthermore, the model assumes a constant ice thickness through time. Even though small variations in the ice thickness through time will affect the absolute value of the reconstructed accumulation rates, the assumption of constant ice thickness is fair for the center of the EAIS where modeled ice thickness variations have been reported up to 200 m (**??**) and is commonly assumed in ice core chronology reconstructions.~~

2.4 ECMWF ERA40 snow precipitation rate

The snow accumulation rates in the Dome C region result from precipitation in the form of snow (snowfall and diamond dust), then modified by wind-driven processes. The wind erosion, wind redistribution and sublimation, as well as other processes during or after a precipitation event, leads to ~~a~~ spatial deposition at the surface that is much less homogeneous than the original precipitation (e.g., **?**). To compare large-scale patterns of precipitation to independent measurements, ECMWF (European Center for Medium-Range Weather Forecasts) ERA40 re-analysis data (**?**) is used to obtain a map of present-day estimated precipitation rates over the survey region. The ECMWF ERA40 model seems to correctly reproduce the observed precipitation's spatial and temporal variability at Dome C, but systematically underestimates the precipitation magnitudes (**??**), probably because clear-sky precipitation is not adequately parameterized (**??**). The ECMWF ERA40 model does not reproduce snow accumulation because it does not consider the blowing snow transport/sublimation process. However, since the Dome C site is not influenced by strong winds, this is expected to have a mi-

nor effect within the summit area, but cannot be completely neglected farther than 25 km from the dome/ice divide. ECMWF ERA40 data have been normalized using the surface accumulation average of the last centuries from existing ground-penetrating radar (GPR) within 25 km from Dome C summit (**?**).

A number of steps went into ~~creating this data set,~~ adjusting the ECMWF ERA40 modeled precipitation rates to field measurements, to calculate the "ECMWF ERA40 estimated present-day surface accumulation rates", shown in Fig.5. These steps are:

1. ECMWF ERA40 monthly average precipitation rates were used to calculate a long term precipitation average over the 1989 - 2011 period
2. Precipitations were then interpolated over the region of interest as a 1 km grid
3. Precipitation values were increased by 12.9 mm yr^{-1} to match GPR measurements in the area (**?**) as ECMWF ERA40 precipitation values are systematically too low compared to ground-based measurements.

Independent traverse accumulation measurements confirm the calculated accumulations (Emmanuel Le Meur, pers comm.)

2.5 Detrending paleoaccumulation rates

To look at small-scale paleoaccumulation variations more closely, we remove large-scale precipitation gradients (see Sect.4). For this, we calculate a quadratic fit of the ECMWF ERA40 present-day surface accumulation values (calculated as described above) with each isochrone-bounded layer's paleoaccumulation, and subtract the calculated fit from the layer's paleoaccumulation values. The result is a map of detrended paleoaccumulations for each isochrone-bounded layer (Fig.6).

2.6 Slope and Curvature in the Prevailing Wind Direction (SPWD and CPWD)

In Sect.4, we discuss the importance of surface slope in the prevailing wind direction (SPWD) and curvature in the prevailing wind direction (CPWD). We use ECMWF 5-year average wind directions (**?**) and **?** surface elevations to calculate SPWD and CPWD values over a 3 km radius in the survey region (Fig.6). A positive value of surface curvature indicates a surface trough, while a negative value of surface curvature indicates a surface bump.

3 Results

We use a standard MH algorithm to run the pseudo-steady ice flow model to invert for time-averaged $\bar{a}$, p' and G_0. Values of the time-averaged $\bar{a}$, p' and G_0 and their uncertainties are obtained after 1000 MH iterations, each taking 5 thermo-mechanical iterations (see companion paper, **?**). **?** describe the

results obtained and the parameter priors used for the inversion. Here, we focus on the accumulation rate reconstructions $\bar{a}$, and $a_{o,\Delta\chi}$ ~~for each isochrone-bounded layer,~~ obtained using Eq.4.

The reconstructed paleoaccumulations $a_{o,\Delta\chi}$ are shown in the top panel of Fig.2 along the A-A' radar transect (VCD/JKB2g/DVD01a) marked on Fig.1. Ages given are the mean of the age interval represented in each paleoaccumulation rate. The A-A' radar line runs along the ice divide, and a marked decreasing ~~gradient~~ accumulation rate can be seen going from the northeast side towards the southwest consistently over all age intervals. Bottom panel of Figure 2 displays $a_{o,\Delta\chi}$ along the B-B' radar transect (OIA/JKB2n/Y77a) marked on Fig.1. This transect runs across the divide and there is no clearly visible ~~accumulation gradient over time for most isochrone-bounded layers~~spatial accumulation gradient for all age intervals, except a ~~weak~~ weaker one for the interglacial 10 ka ~~and 128 ka isochrones.~~ isochrone. This is expected as the southern end of this radar line is on the high-accumulation side of the divide.

We also show reconstructed accumulation rates in map view in Fig.3 and 4. Fig.3 displays the time-averaged accumulation rate $\bar{a}$ and Fig.4 displays the paleoaccumulation rate per isochrone-bounded layer $a_{o,\Delta\chi}$. We show ~~six of the~~ all four age intervals calculated. We observe that the time-averaged accumulation (Fig.3) has a clear north to south gradient, decreasing from $>$ 21 mm water equivalent per year (mm-we yr^{-1}) in the north to 15 mm-we yr^{-1} in the south. Superimposed, we observe a number of regions ~20 km wide that show a ~25% accumulation increase over the ~~LDCm, to~~ LDCM, to ~50 km wide or more east of the CR with a ~75% increase~~over the CR~~. These are outlined by black lines on Fig.3. Around the CR, we also note that the extended area of high accumulation is ~~preceded by~~ adjacent to an area of very low accumulation, parallel to it and just east of the CST. This corresponds to an area of drastic surface slope and curvature change (see also Fig.6, ~~Sect.4 and~~ S3, and S4).

~~Paleoaccumulation~~ The spatial pattern of paleoaccumulation rates per isochrone-bounded layer (Fig.4) ~~show a similar pattern in the accumulations~~is similar to that of the time-averaged accumulation: a large-scale gradient N-S with superimposed areas of higher accumulation in the same locations as ~~in~~ for the time-averaged accumulation reconstruction. We note a striking similarity between the time-averaged accumulation rate (Fig.3) and the paleoaccumulation rates for the ages 0 ka - ~~38~~ 10 ka (Fig.4). We also note that ~~gradients are stronger for interglacial age intervals~~ accumulation rates are higher for the interglacial age interval (0 ka - 10 ka~~and 121 ka - 128 ka in~~) than for the glacial age intervals (see Fig.4 and S4). The small-scale accumulation patterns ~~remain spatially stable through time: panels in Fig.4 ranging from~~ are visible in the 0 ~~ka to 106 ka display these~~ - 10 ka age interval, we see the same three areas of high accumulation as outlined in Fig.3. ~~The areas are ~20 kilometers wide and ~50 km or more east of the CR. However, they are less prominent on the 121 ka - 128 ka panel on Fig.4, except for east of the CR~~For older layers, the smaller spatial extent of the paleoaccumulation data makes it difficult to conclude on the persistence of these small-scale high accumulation areas.

~~Also plotted on Fig.3 and 4 are bedrock~~ Bedrock elevations from Bedmap2 (**?**) augmented with new OIA survey data outlined with a dashed rectangle (**?**), as well as **?** surface elevation contours~~.~~ , are plotted in the background of Fig.3 and 4. The areas of higher accumulation are co-located with areas of low surface slopes, visible from the surface contours. The accumulation variations we observe are also co-located with significant bedrock relief changes, which reach e.g. ~2000 m for the CR escarpment, and ~500 m for the south side of the ~~LDCm~~ LDCM (see Fig. S1).

We use the time-averaged accumulation, $\bar{a}$, obtained from the model and Eq.1 to plot Holocene average accumulation rates. For this, we take the ratio of the average accumulation rate of the last 100 years to that of the last 800 kyrs using the AICC2012 chronology, which has a value of 0.65. The time-averaged $\bar{a}$ is scaled by this factor of 0.65 to obtain Holocene average accumulation rates, which we call a_{100yrs} here. We plot a_{100yrs} together with ECMWF ~~ERA40-based precipitation~~ ERA40-derived surface accumulation data in Fig.5 (see Sect.2.4 for details). We observe that the large-scale N-S accumulation gradient in a_{100yrs} closely resembles that of the ECMWF ERA40-derived surface accumulation rate in Fig.5: high accumulation in the north nearer the coast, and lower accumulation in the south as you move towards the interior. The magnitude of the accumulation rates also ~~match~~ matches surprisingly well.

The calculated accumulation rate uncertainties from the model, with an average value of 0.16 mm-we yr^{-1} (see Fig. S2), are an order of magnitude (or more) smaller than the values of reconstructed time-averaged accumulation rate, providing confidence in the time-averaged accumulation rates calculated. However errors have been treated as uncorrelated so we cannot apply these uncertainties to the paleoaccumulations. We hope to improve this in the future.

To focus on the small-scale variations in paleoaccumulations, we plot detrended paleoaccumulations (see Sect.2.5) for the region on top of SPWD and CPWD values (see Sect.2.6), as shown on Fig.6. ~~As a reminder, these accumulation maps therefore display values of detrended paleoaccumulation once the large-scale precipitation gradient obtained from ECMWF ERA40 has been removed~~We only show this relationship for the first layer, spanning the past 10 kyrs, as older layers are not as extensive. Looking at the spatial distribution of these detrended paleoaccumulations in relation to SPWD, we observe that areas with high accumulation are co-located with areas of markedly reduced SPWD values with respect to the surrounding values (~0.5-1.2 x 10^{-3} of absolute SPWD decrease~~).~~ ~~This is displayed in~~ , see Fig. S3). But more striking is the clear relationship between the magnitude of the curvature (and polarity) and the magnitude of the residual paleoaccumulation (Fig.6). ~~Areas of high~~ The areas of high accumulation in Fig.3 are outlined in black. They correspond to areas of high positive detrended paleoaccumulation, $>$ 1.2 mm-we yr^{-1}, and are well correlated with areas of strongly positive curvature values ($>$ 2 x 10^{-7} m^{-1}). This is evident in the ~~LDCm areafor the high accumulation areas highlighted on Fig. 3.~~ LDCM area. Areas of high negative detrended accumulation, $<$ -1.6 mm-we yr^{-1}, are also well correlated with areas of strongly negative curvature. This is best seen east of the CR. ~~Note that the~~ The correlation holds particularly well for the youngest layer

(0 - 10 ka) ~~; the residual paleoaccumulation values east of the CR are high directly where the surface curvature is strongly positive, low where the surface curvature is strongly negative (blue on blue, red on red on Fig. 6). However, for layer~~ over the entire region. We plot detrended paleoaccumulation for layers older than 10 ~~- 38 ka and older, this relationship is slightly offset, best visible east of the CR area.~~ ka, and observe that this relationship holds over the LDCM, with a slightly increasingly offset with increased ages (see S4).

4 Discussion

The 1D assumption to calculate paleoaccumulation rates is clearly the largest source of uncertainty in our reconstructions. In the 1D pseudo-steady ice flow model described in the companion paper (**?**), the goal is to constrain the age of the deep ice. For that work, trade-offs in the strain thinning (i.e. p and G_0) and accumulation rates do not matter, as their combined effects dictate the age of the ice. However, to calculate the layer-by-layer paleoaccumulation rates, we have to assume that τ (Eq.4) is fitted perfectly, which breaks down as horizontal advection increases. We reckon that for the first layer whose average depth is ~150 m, that is ~5% of the total depth, the error in the thinning is small enough to not pollute significantly our accumulation results (total thinning is always above 0.9). For the other layers, it is difficult to imagine an error in the thinning function that would produce, by chance, a similar accumulation pattern to that of the first layer. In addition, by setting a limit on the maximum horizontal advection allowed for each age interval, the described accumulation patterns and variations are reasonably unaffected by the 1D assumption. The threshold of 5 km is chosen such that horizontal advection is negligible compared to the scale of the observed accumulation rate variability. The small-scale areas of high accumulation are at least 20 km wide in the region, therefore the 5 km threshold on horizontal movement does not affect our conclusions. We are only able to reconstruct paleoaccumulation rates back through 73 ka, therefore a 3D model is required to look at paleoaccumulation rates further back in time.

Furthermore, the model assumes a constant ice thickness through time. Even though small variations in the ice thickness through time will affect the absolute value of the reconstructed accumulation rates, the assumption of constant ice thickness is fair for the center of the EAIS where modeled ice thickness variations have been reported below 200 m (**???**) (representing a 5% error on the ice thickness), and little is known of the spatial distribution of these ice thickness variations in the center of the ice sheet. A 5% error on the ice thickness will produce a 5% error on the thinning function τ (**?**) and therefore a 5% error on the accumulation rates calculated. This error can be ignored for two reasons. First, it is small compared to the accumulation variations that we observe (larger than 10%). And second, it only affects the absolute value of the accumulation rates reconstructed but not the relative differences in accumulation rates from one location to the next in the Dome C region. Since we focus exclusively on changes in gradients and patterns in accumulation rates, this additional

source of error doesn't affect our conclusions. Despite this error, we observe a clear reduction in the magnitude of the accumulation rates as we go back in time and enter the last glacial maximum, as expected and measured in ice cores (**???**).

The observed patterns of paleoaccumulation agree well with previous studies of surface snow accumulation variability in the Dome C region. Considering first the large-scale patterns in the accumulation reconstructions~~(Fig.3 and 4)~~, we observe a consistent large-scale gradient ~~for each age interval. Large-scale~~ (large-scale here refers to 100s of kilometers~~. Accumulation decreases~~) for each age interval, with accumulation values decreasing from the north side of Dome C to the south side. ~~This is~~ **?** suggest moisture provenance from the Indian Ocean sector is the most consistent with the clear north south gradient in precipitation observed as we near Dome C. The fact that our paleoaccumulation reconstructions reproduce the present-day large-scale surface accumulation gradient and that this remains true back to 73 ka suggests persistence of the source of moisture for this part of the East Antarctic plateau through the last glacial and deglaciation. Transects A-A' and B-B' in Fig.2 clearly show the north south orientation of the accumulation gradient. This large-scale accumulation gradient is also clearly seen in the ECMWF ERA40 data for the region (~~see~~ Fig.5)~~. Other large scale~~ , as well as in other large-scale accumulation models of the region (e.g. **?**) or Regional Climate Model (MAR) (**??**)~~also display such accumulation patterns~~. GPR data collected during traverses across Dome C and along the divide also show a ~~clear N-S~~ strong north-south gradient in accumulation ~~(??, Emmanuel Le Meur, pers. comm).~~ (**??**, Emmanuel Le Meur, pers. comm.). We note a good agreement between our accumulation values and trends along A-A' going from Dome C along the ice divide towards Vostok (top panel of Fig.2) and the GPR transect measured by **?** on the other side of the Dome C divide. A SPRI airborne transect collected over Dome C ~~also~~ shows a strong accumulation gradient of 10s of mm yr^{-1} over a spatial scale of 100s of km (**?**).

~~The fact that our paleoaccumulation reconstructions reproduce present-day surface accumulation gradients and that this remains true back to 128 ka suggests both a stable meteorologic system and location of Dome C. To preserve the same N-S gradient , the moisture-bearing air masses coming from the coast must have interacted with the same surface topography during those 128 kyrs~~**?** show a small component of counter-clockwise rotation of the accumulation pattern in historical times centered on Dome C, but the general north south gradient difference in accumulation across the dome remains. Measurements made in other areas of the ice sheet, e.g. across Talos Dome (**?**), point to similar patterns: accumulation is highest near the moisture source and decreases with distance from the coast. **?** point to the same patterns of reduced accumulation inland across Dronning Maud Land. ~~Such a consistent large-scale depositional pattern indicates a stable regional topography of the Dome C region. **?** show a small component of counter-clockwise rotation of the accumulation pattern in historical times centered on Dome C, but the general N-S gradient difference in accumulation across the dome remains. We note a good agreement between our accumulation values and trends~~

along A-A' going from Dome C along the ice divide towards Vostok (top panel of Fig.2) and the GPR transect measured by ? on the other side of the Dome C divide.

Considering the small-scale (10s of kilometers or a few ice thicknesses) patterns of accumulation shown earlier, we described several regions of locally higher increased accumulation. The co-location of the areas of higher accumulation with areas where surface slope is reduced, as seen from the surface contours or the markedly reduced SPWD values with respect to the surroundings (Fig. S3), fits well with the model put forward by ?over Talos Dome where . ? show that accumulation increases when SPWD decreases . They over Talos Dome and attribute the correlation between the absolute magnitude of SPWD and accumulation rates to katabatic wind-driven ablation. Note that the prevailing wind direction over the area is more or less along the long axis of Dome C flowing from higher up the ice divide towards Dome C (??)(see Fig.6, ??).

The spatial correlation we obtain between the detrended paleoaccumulations and the CPWD can be explained by the same mechanisms as for SPWD, since SPWD and CPWD are directly related. The proximity of the isochrone-bounded layer to the surface influences how well the correlation holds, particularly visible in the CR region. Layer 0 - 10 ka shows high detrended paleoaccumulation values where the surface curvature is strongly positive (i.e. surface trough), and low values where the surface curvature is strongly negative (i.e. surface bump). This is true for both the LCDM and CR regions. The proximity of the isochrone-bounded layer to the surface influences how well the correlation holds, particularly visible in the CR region which is furthest from the divide. For any deeper layer (Fig.S4), this relationship is slightly offset in space. This could be due to ice flow increasing with distance from the dome. Accumulation rates are calculated using radar isochrones at depths between ~9% and 53% of the ice thickness at Dome C. Therefore, we expect that a strongly positive CPWD region would affect the accumulation rate directly above this same region. These anomalies are preserved by progressive burial and as ice flow speed over the CR relief is higher than over the LDCm, radar isochrones observed at the CR will have carried this anomalous accumulation signature further down-flow than they would have at the LDCm; a likely cause is the increased amount of horizontal advection with depth, up to the set maximum of 5 km .

Even though the absolute magnitudes of slope and curvature changes we observe are relatively small (on the order of 10^{-3} and 10^{-7} m^{-1}, respectively), other studies have shown that even very small slope changes can have a strong influence on wind-borne redistribution of snow (??)(???). However a single mechanism has yet to be described that would explain the relationship between CPWD (and therefore SPWD) and small-scale accumulation variations. ? observe strong surface density variations linked to surface slope breaks, however some increases in accumulation occur over steeper surface slopes, which is surprising when steep slopes are usually associated with reduced accumulation (??). ? show that local slope changes of 0.01 can create up to 30% variations in accumulation, and invoke a highly non-linear relationship between wind speed and snow transport to explain the type of accumulation variability they observe. ? also shows that slope changes as small

as 0.001 over a distance of 3 km can affect snow deposition, and argues for a relationship between slope, wind strength and mass drift drift transport.

The extreme pattern of high and low accumulation parallel to the CST and east of the CR seems to be the ideal example of how surface topography variations affect accumulation rates. The ice flowing radially away from Dome C has to flow over the CST and the prominent bedrock CR. CPWD shows strongly negative values over the subglacial CR; it creates a surface which is concave down perpendicular to the wind direction. We can imagine a scenario in which snow is strongly plucked away on this steepest surface slope, but further down-wind, as slope reduces and reaches contrastingly strongly positive CPWD, the snow can then be redeposited directly down-wind as suggested in **?**.

We attempted a series of low order (linear and quadratic) fits between CPWD and our detrended paleoaccumulations but none explain all the variability. The data is suggestive of threshold behaviors between low and high CPWD magnitudes. ECMWF wind speed magnitudes over the ~~LDCm~~ LDCM and CR areas (**?**) are below the 5 m s^{-1} threshold for dune processes to be active in the region, and the radar data used ~~does~~ do not show any buried dune structures. The accumulation patterns observed are more suggestive of the preferential infill of surface troughs by winds. These troughs might not fill-up easily because of the very low surface precipitation rates in the region (**??**) combined with the presence of areas of subglacial melting in the region (**?**), creating additional draw-down of the surface.

~~Although we cannot yet explain the mechanisms causing the small-scale paleoaccumulation variability we observe in the Dome C region, our results have important ramifications for constraining the region's stability through time. If we assume slope morphology in the prevailing wind direction is the dominating control on accumulation variability, the temporal persistence of the patterns of accumulation is only possible if the surface morphology, i.e the SPWD and CPWD, is also spatially unchanging, independent of whether the control comes from the bedrock topography. If the surface slope and curvature do not change, we can suppose this implies the position of the divide and the dome must have remained relatively stable. This implies that the present-day configuration of the ice sheet in the region could have been the same through the last 128 kyrs. Geometric information on Dome C and its surrounding region is critical and so far unconstrained in climate reconstructions of the EAIS. Dome C and the surrounding ice divides have long been modeled as stable spatially but this hypothesis has lacked evidence. The results shown here provide the first piece of such evidence.~~

~~Note the extreme pattern of high and low accumulation parallel to the CST and east of the CR seems to be the ideal example of how surface topography variations affect accumulation rates. The ice flowing radially away from Dome C has to flow over CST and over the prominent bedrock CR. CPWD shows strongly negative values over the subglacial CR; it creates a surface which is concave down perpendicular to the wind direction. We can imagine a scenario in which snow is strongly~~

plucked away on this steepest surface slope, but further down-wind, as slope reduces and reaches contrastingly strongly positive CPWD, the snow can then be redeposited directly down-wind as suggested in **?**.

We noted in the results that the small-scale accumulation variations were co-located with bedrock relief variations (see Fig. S1). **?** explain that bedrock topography can be the underlying influence on the variability of snow accumulation at scales of 1-20 km, corresponding to the lengthscales of the accumulation variations we calculate here. Bedrock topography will have a stronger influence on the overlying ice in the presence of subglacial lubrication (**?**). **?** show that for the Dome C region, the most positive surface curvatures are directly linked to the largest ice thicknesses and the presence of subglacial lakes. It is interesting to note that areas of higher detrended paleoaccumulation correlated to high positive CPWD in this study outlined in Fig.3 are above deep bedrock valleys dotted with many observed subglacial lakes (**?**). One interesting area is the band of high positive curvature highlighted on Fig.6 with a black arrow. Here we observe a band of high detrended paleoaccumulation between 0 - 73 ka intervals, but not in the 73 - 82 ka interval. It seems instead to get displaced further west. Ice here is resting in a shallower valley with limited subglacial lakes. The difference in behavior could be linked to transient freezing of the bedrock in regions of thinner ice which would lead to transient surface topography.

Small-scale accumulation patterns appear to be different for Although we cannot yet explain the mechanisms causing the small-scale paleoaccumulation variability we observe in the age interval 121 - 128 ka. This period represents the penultimate interglacial and it is possible surface topography changes occurred in the Dome C region. However, we do not attempt to further explain these changes because this layer is at a depth of ~50% of the ice column where the 1D inversion is less robust. This will be testable with a 3D model.

More accurate absolute accumulation rates could be obtained using a Dome C region, which is beyond the scope of this manuscript, our observations have important ramifications for better understanding the region's stability through time. In the future, we hope to improve our paleoaccumulation rate reconstructions, and in particular go back further into the last glacial cycle with a full 3D thermo-mechanical model. Further GPR data was recently collected over the LDCmLDCM, and strain nets and various other instruments were have been deployed. These new measurements will allow a test of the accumulation reconstruction of this studyadd to the existing data set and provide important constraints if we hope to develop 3D inversions.

5 Conclusions

We reconstructed accumulation rates for the last 128 73 kyrs. Looking at both large- and small-scale accumulation gradients, we show that these have not changed significantly over since the last glacialcycle. Large-scale accumulation gradients will remain constant if moisture-bearing air

mass ~~trajectories~~ trajectory interactions with surface topography do not vary~~, which means that the topographic controls must remain unchanged~~. Small-scale accumulation variations are strongly controlled by SPWD and CPWD and therefore, if the pattern of high and low accumulations remains fixed over a long period of time, this requires consistent interactions between local surface slopes and prevailing winds over the last ~~128~~ 73 kyrs, independent of whether the control comes from the bedrock topography and/or potential basal melting. ~~Both suggest that the current surface topography of the Dome C region has not changed significantly over the last glacial cycle.~~ This points to a ~~stable position of~~ spatially stationary and persistent accumulation pattern in the Dome C region ~~and adjacent ice divides~~over the last glacial, an important constraint for modeling efforts in the area, both for dating existing ice cores as well as for the prospecting of a ~~greater than 1~~ 1.5 million-year-old ice core site.

6 Data accessibility

The radar isochrones used in this manuscript will be made publicly available in ~~summer 2017~~ 2018 as a separate publication. Code for the model is available publicly under https://github.com/parrenin/IsoInv.

7 Author contributions

M.G.P. Cavitte interpreted and analysed the radar isochrones, F. Parrenin developed the model and ran experiments with M.G.P. Cavitte with C. Ritz input, D.A. Young, J.L Roberts and D.D. Blankenship were involved in survey design and data acquisition, B. Van Liefferinge and M. Frezzotti provided data and discussion material. M.G.P. Cavitte prepared the manuscript with contributions from all co-authors. The authors declare that they have no conflicts of interest.

Acknowledgements. This ~~research~~ publication was generated in the frame of Beyond EPICA-Oldest Ice (BE-OI). The project has received funding from the European Union's Horizon 2020 research and innovation programme under grant agreement No. 730258 (BE-OI CSA). It has received funding from the Swiss State Secretariate for Education, Research and Innovation (SERI) under contract number 16.0144. It is furthermore supported by national partners and funding agencies in Belgium, Denmark, France, Germany, Italy, Norway, Sweden, Switzerland, The Netherlands and the United Kingdom. Logistic support is mainly provided by AWI, BAS, ENEA and IPEV. The opinions expressed and arguments employed herein do not necessarily reflect the official views of the European Union funding agency, the Swiss Government or other national funding bodies. This research was made possible by the joint French–Italian Concordia Program, which established and runs the permanent station Concordia at Dome C. This work was supported by NSF grants ANT-0733025~~and~~, ARC-0941678, and PLR-1443690, NASA grants NNX08AN68G, NNX09AR52G, and NNX11AD33G (Operation Ice Bridge) to Texas, the Jackson School of Geosciences, the Gale White UTIG Fellowship, the G. Unger Vetlesen Foundation, NERC grant NE/D003733/1, the Global Innovation Initiative award from the British Council,

the Australian Government's Cooperative Research Centre's Programme through the Antarctic Climate and Ecosystems Cooperative Research Centre (ACE CRC). Operational support was provided by the U. S. Antarctic Program and by the Institut Polaire Français Paul Emile Victor (IPEV) and the Italian Antarctic Program (PNRA and ENEA) and the Australian Antarctic Division provided funding and logistical support (AAS 3103, 4077, 4346). We acknowledge the support of Kenn Borek Airlines. Additional support was provided by the French ANR Dome A project (ANR-07-BLAN-0125), the CNRS/INSU/LEFE fundings "IceChrono" and "CO2Role" and the Grenoble-Alpes University AGIR funding "Oldest Ice". Special thanks to Dr. Olivier Passalacqua for fruitful discussions. This is BE-OI publication number ####. This is UTIG contribution 3116.

Table 1: Radar isochrones and their uncertainties at the Dome C ice core site.

Isochrone	
1	
2	
3	
4	

5 1171.90 3.18 82.01 1.55 **6** 1337.90 3.78 96.49 1.74 **7** 1446.80 3.97 106.25 1.83 **8** 1593.90 4.32 121.09 1.70 **9** 1682.10 4.51 127.78 1.78 height

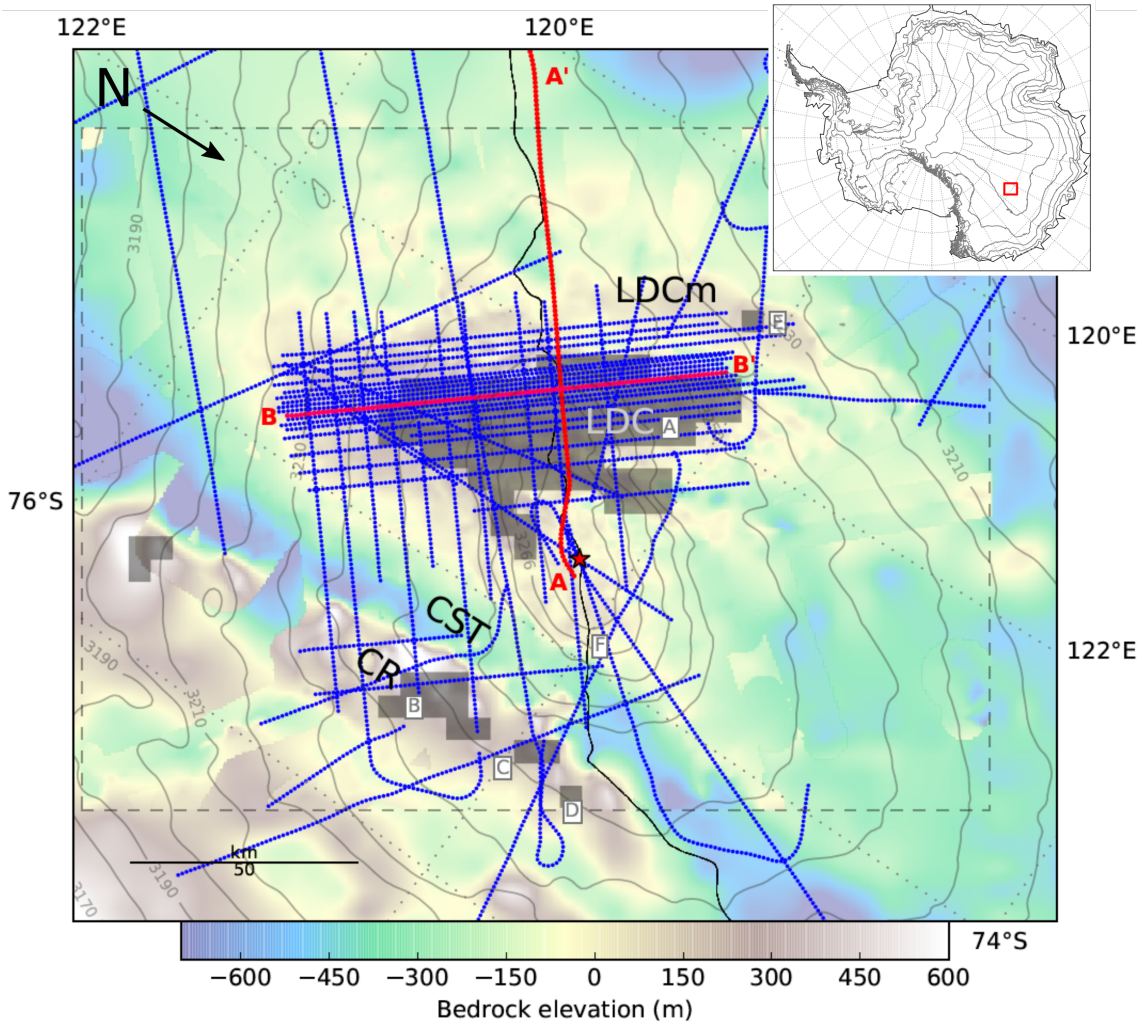

Figure 1: Map of Dome C and the surrounding region. A red square locates the study area on the inset. The radar lines used in the accumulation reconstructions are displayed as blue lines. Highlighted in red are the two radar lines shown in Fig.2. Dark gray blocks labeled A-E are the **?** Candidate regions. F labels a 1.5 million-year-old ice new Candidate site (see companion paper). The background is bedrock elevation in meters above sea level and combines Bedmap2 bed elevations (**?**) as well as a recompilation based on the OIA radar bed elevations (**?**) delimited by a dashed rectangle (elevation differences are particularly visible along the CR). Gray ~~lines~~ contours are **?** surface elevations, a black line locates the ice divide. A red star locates the EPICA Dome C ice core. LDC locates the gentle secondary surface dome, ~~LDCm~~ LDCM locates the Little Dome C massif under the densest radar lines, CR locates the Concordia Ridge steep escarpment along the Concordia Subglacial Trench (CST).

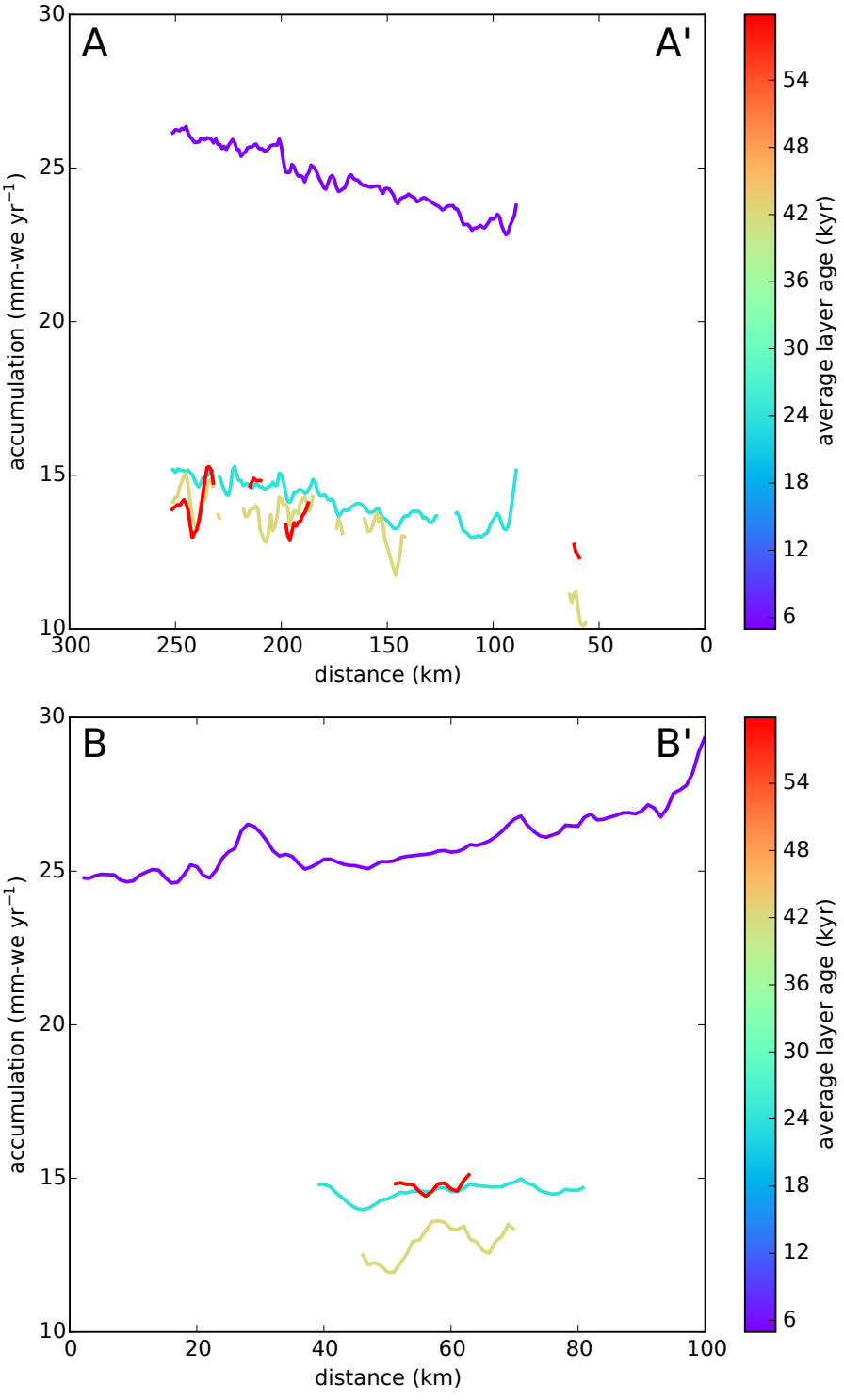

Figure 2: Paleoaccumulation rates along radar lines. Colors represent the mean of the age interval $\Delta\chi$ ~~represented by~~ for each layer. Top panel shows the reconstructed paleoaccumulation rate $a_{o,\Delta\chi}$ along the A-A' radar line. Bottom panel is along the B-B' radar line. Both radar lines are highlighted on Fig.1, distance represents kilometers along each radar line. Results are filtered to remove regions of excess horizontal strain. A-A', along the ice divide, displays a strong and consistent accumulation gradient. B-B', perpendicular to the ice divide, shows no ~~similar~~ gradient except a weaker one for the interglacial 10 ka isochrone on its southern edge.

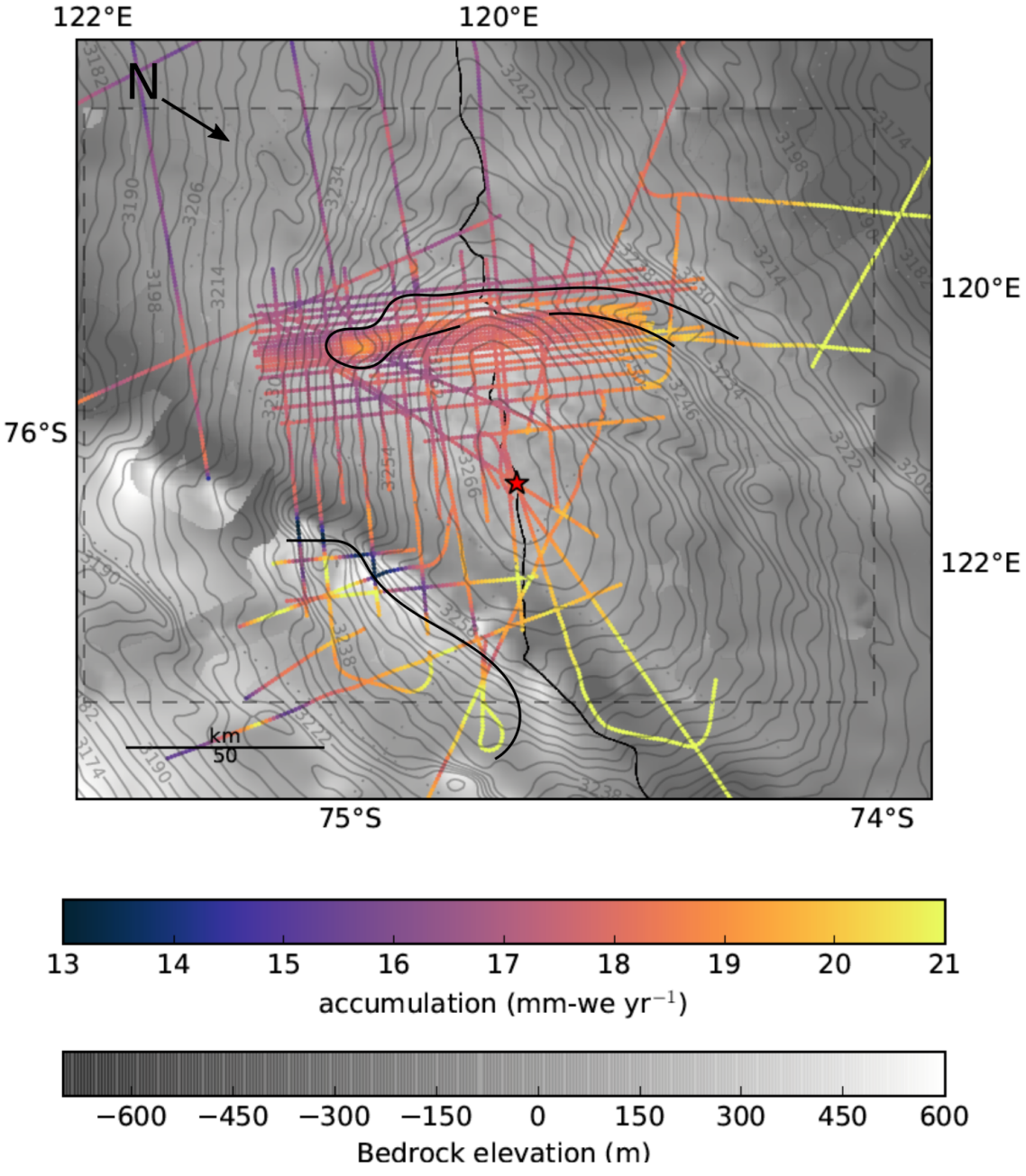

Figure 3: Time-averaged accumulation rates $\bar{a}$ along the radar lines over the Dome C region. Accumulation rates are given in mm of water equivalent per year. There is a clear large-scale N-S accumulation gradient, with accumulation decreasing with distance from the Indian Ocean coast, the main pathway of snow precipitation. Black lines outline areas of small-scale high accumulation: they correlate to areas where surface contours (in gray) become further apart, i.e. where surface slope is reduced. Background is the same as in Fig.1.

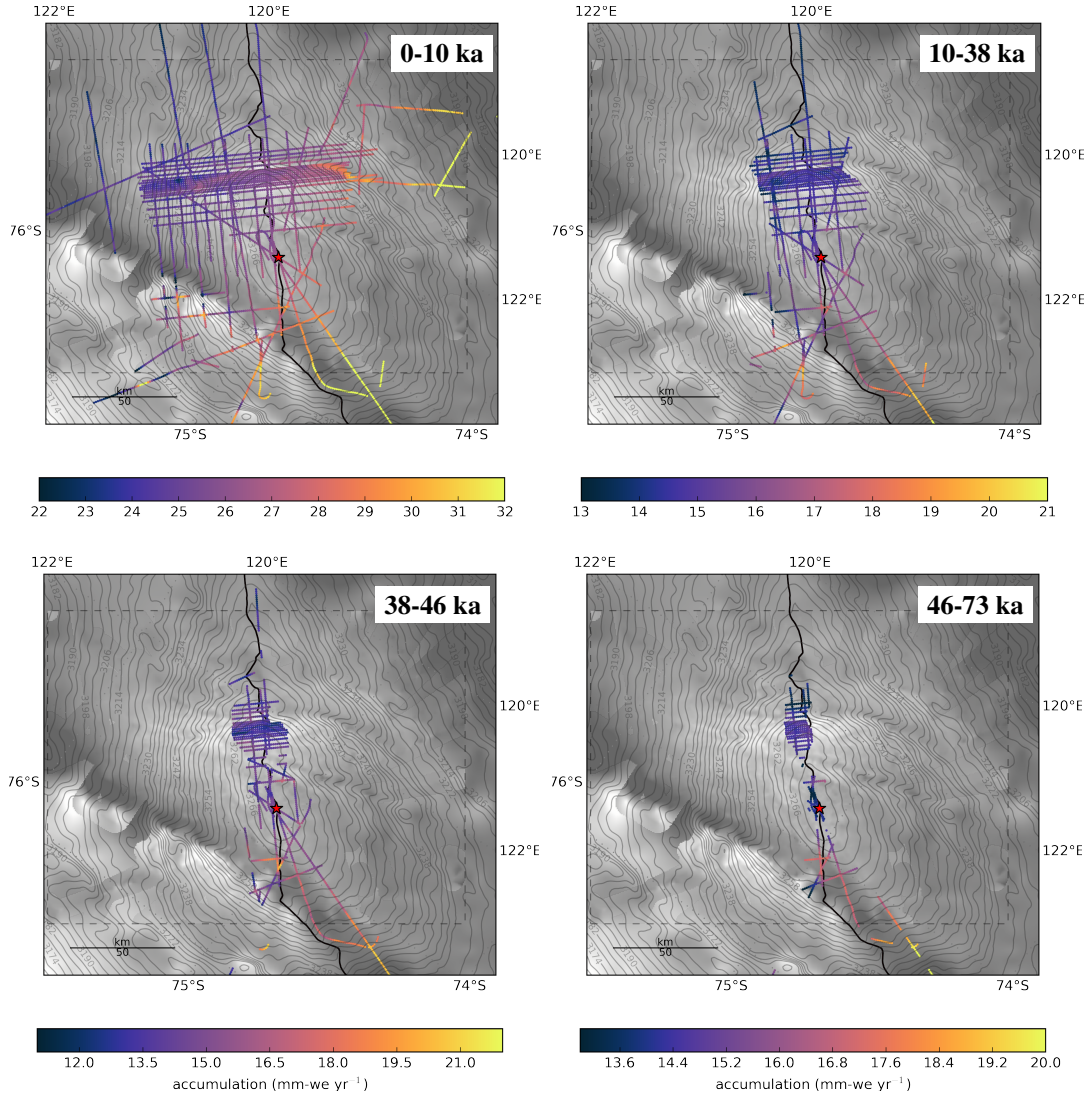

Figure 4: Paleoaccumulation reconstruction over the Dome C region since 73 ka. Panels show paleoaccumulation rates calculated for each isochrone-bounded layer, age intervals are given on each panel. Results are filtered to remove regions of excess horizontal strain. The north south accumulation rate gradient, decreasing with distance from the Indian Ocean coastal sector, remains stable for the last 73 ka. Background is the same as in Fig.1.

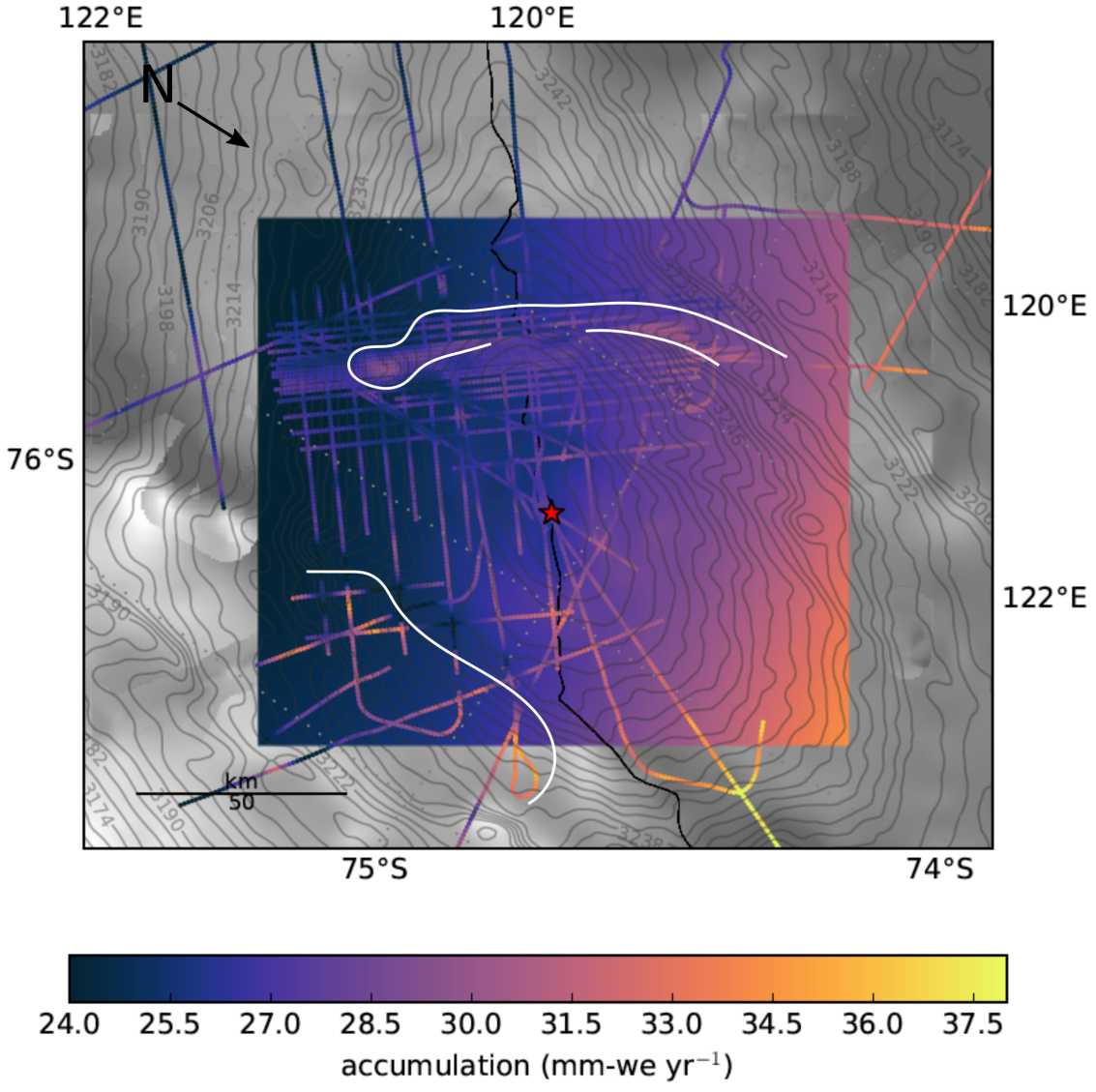

Figure 5: Holocene average accumulation rates a_{100yrs} along the radar lines superimposed on ECMWF ERA40 estimated present-day surface accumulation rates (see Sect.2.4). There is a very good agreement in the magnitude of accumulation values between the two datasets and in their ~~N-S~~ north south accumulation gradient on large-scales (100s km), with accumulation decreasing with distance from the coast. White lines outline the same areas of small-scale high accumulation as in Fig.3. Background is the same as in Fig.1.

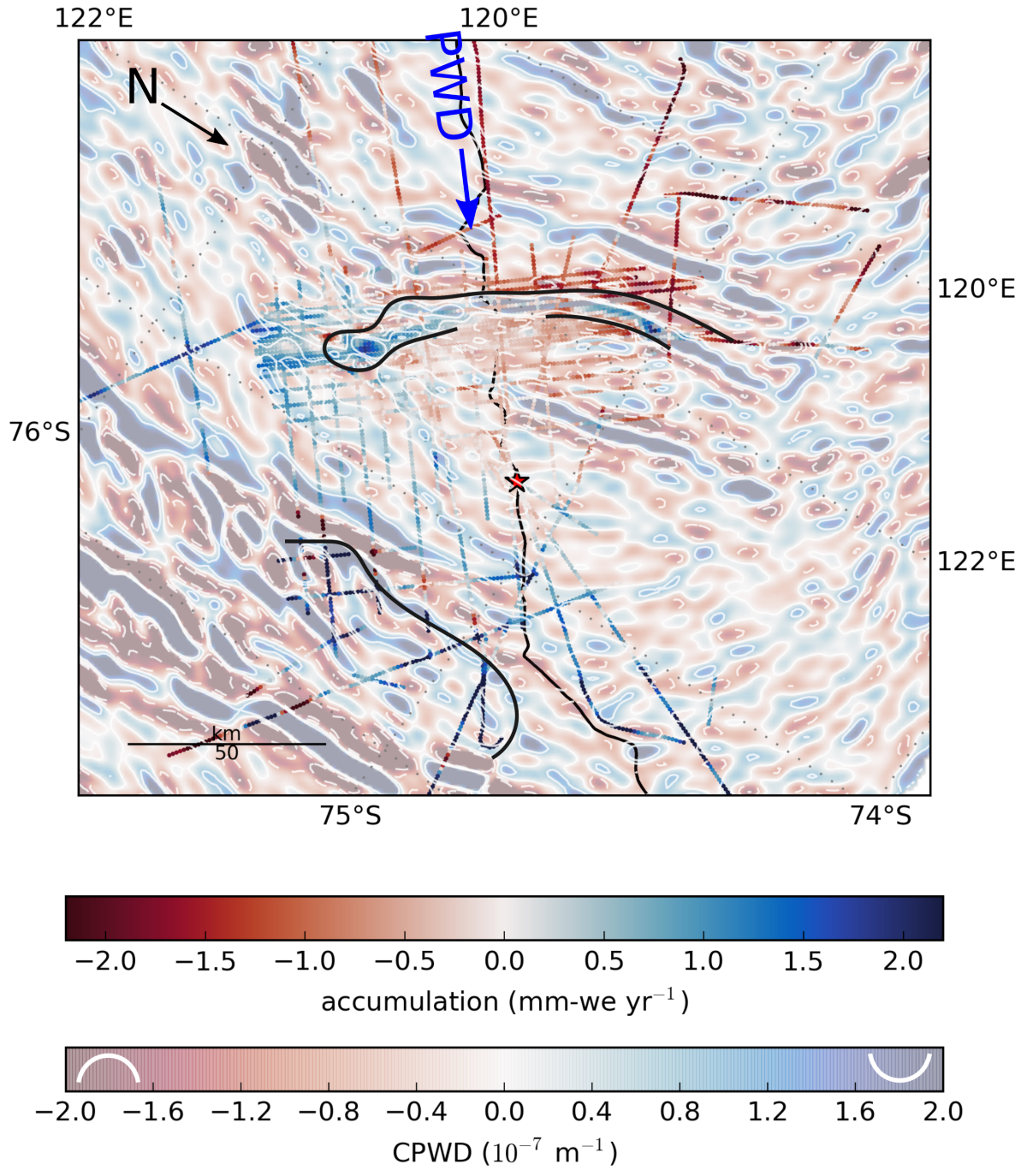

;;;;;;

Figure 6: Residual paleoaccumulations over the region for the 0 - 10 ka age interval, overlain on surface curvature in the prevailing wind direction (CPWD, strongly positive and negative values are sketched on either end of the colorbar). Black lines outline the same areas of small-scale high accumulation as on Fig.3 and 5. Results are filtered to remove regions of excess horizontal strain. The residual paleoaccumulation highs correlate well to areas of strongly positive CPWD. A blue arrow indicates prevailing wind direction.